Synthesis, thermionic emission and magnetic properties of $(Nd_xGd_{1-x})B_6$*

Bao Li-Hong(包黎红)[a], Zhang Jiu-Xing(张久兴)[a]†,
Zhou Shen-Lin(周身林)[a], and Tegus(特古斯)[b]

[a] *Key Laboratory of Advanced Functional Materials of Ministry of Education, College of Materials Science and Engineering, Beijing University of Technology, Beijing* 100124, *China*

[b] *Inner Mongolia Key Laboratory for Physics and Chemistry of Functional Materials, College of Physics and Electron Information, Inner Mongolia Normal University, Hohhot* 010022, *China*

(Received 27 November 2010; revised manuscript received 17 January 2011)

Polycrystalline rare-earth hexaborides $(Nd_xGd_{1-x})B_6$ ($x = 0$, 0.2, 0.6, 0.8, 1) were prepared by the reactive spark plasma sintering (SPS) method using mixed powder of GdH_2, NdH_2 and B. The effects of Nd doping on the crystal structure, the grain orientation, the thermionic emission and the magnetic properties of the hexaboride were investigated by X-ray diffraction, electron backscattered diffraction and magnetic measurements. It is found that all the samples sintered by the SPS method exhibit high densities (> 95%) and high values of Vickers hardness (2319 kg/mm^2). The values are much higher than those obtained in the traditional method. With the increase of Nd content, the thermionic emission current density increases from 11 to 16.30 A/cm^2 and the magnetic phase transition temperature increases from 5.85 to 7.95 K. Thus, the SPS technique is a suitable method to synthesize the dense rare-earth hexaborides with excellent properties.

Keywords: rare-earth hexaborides, spark plasma sintering, emission property

PACS: 81.05.Je, 61.66.Fn, 75.50.Ee **DOI:** 10.1088/1674-1056/20/5/058101

1. Introduction

Rare-earth hexaborides with simple cubic CaB_6-type structure have attracted great interest owing to their special electronic and magnetic properties. Among the rare-earth hexaboride families, LaB_6[1−3]as an electron source shows high brightness, low vapor pressure and chemical stability at elevated temperatures, and a favorable work function. Compared with LaB_6, CeB_6[4,5] has a lower work function (2.5 eV), a lower operation temperature and a higher electrical resistance, thus is a more suitable material for the direct heating thermionic electron emitter. The CeB_6 is a dense Kondo material and shows heavy fermion behaviours.[6] NdB_6[7] and GdB_6[8,9] are extensively studied due to the complicated magnetic transport properties. The NdB_6 orders in an A-type antiferromagnetic structure below $T_N \approx 8$ K and the GdB_6 has two magnetic phase-transition temperatures. However, the thermionic emission properties of NdB_6 and GdB_6 have been rarely reported in the literature so far. In addition, it is difficult to prepare high-density polycrystalline bulks of NdB_6[10] and GdB_6[11] by the traditional solid-phase sintering method, owing to the powder characterization of the high plastic yield stress. Therefore, there are great research prospects for full densification of bulk NdB_6 and GdB_6, especially for obtaining their excellent thermionic emission or field emission properties.

It has been reported[12] that the La element doping into PrB_6 and NdB_6 leads to a reduction of the effective work function. Moreover, these substituted multiple rare-earth hexaborides exhibit better emission performance than LaB_6. Therefore, an appropriate doping of rare-earth element[13−15]can significantly improve the emission property. Based on the above studies, it can be inferred that full densification and an appropriate doping of rare-earth element are essential for obtaining the reproducible and improved properties.

In the present work, the high density polycrystalline GdB_6 are fabricated by the spark plasma reactive liquid phase sintering (SPS) method and the Nd doping effects on structure, grain orientation, thermionic emission and magnetic properties of GdB_6 are investigated.

*Project supported by the National Natural Science Foundation of China (Grant No. 50871002).
†Corresponding author. E-mail: zjiuxing@bjut.edu.cn
© 2011 Chinese Physical Society and IOP Publishing Ltd

2. Experiments

The NdH_2 and the GdH_2 nanopowders were prepared in a mixed gas of hydrogen and argon using the raw material neodymium (99.95% purity) and gadolinium (99.9% purity). The amorphous boron (99.9% purity, 10 μm), the NdH_2 and the GdH_2 nanopowders with fixed molar ratios were mixed in an agate mortar. Finally, the mixtures were placed into a graphite die with inner diameter of 20 mm for liquid-phase SPS processing using a sumimoto SPS-3.20MK-V sintering system. The following conditions were applied for the SPS sintering: The axial mechanical pressure was 50 MPa, the heating rate was 110 °C/min, the sintering temperatures were 1450–1500 °C and the sintering time was 5 min. The synthesis was based on the following chemical reaction:

$$x\mathrm{NdH_2(s)} + (1-x)\mathrm{GdH_2(s)} + 6\mathrm{B(s)} \longrightarrow \mathrm{Nd}_x\mathrm{Gd}_{1-x}\mathrm{B_6(s)} + \mathrm{H_2(g)}. \quad (1)$$

The phase and the compositions of the $(Nd_xGd_{1-x})B_6$ samples were examined by using X-ray diffraction (CuK_α radiation, Bruker D8) and X-ray fluorescence (XRF: Magix PW2403). The powder morphologies were characterized using the transmission electron microscopy (TEM: JEM-2010) and the electron backscattered diffraction (EBSD). The latter investigation was carried out in an FEINANO 200 scanning electron microscope incorporating an EDAX TSL OIM5.2 system. The densities of all sintered bulks were measured by using the Archimedes method and then compared with their theoretical values. Characterization of the electron emission properties was carried out at the University of Electronic Science and Technology of China. The emission area of the cathode was 1 mm^2 in the thermionic emission measurement. The Vickers hardness was measured by using a MICROHARDNESS TESTER FM-700 under a load of 5 N. The magnetic measurements were performed by using a quantum design SQUID magnetometer in the temperature range from 5 K to 300 K.

3. Results and discussion

3.1. TEM images of the NdH_2 and the GdH_2 nanopowders

Figure 1 shows the TEM images of the NdH_2 and the GdH_2 nanopowders fabricated by the arc plasma method. The primary particles of NdH_2 and GdH_2 have nearly spherical morphology with a diameter of about 20 nm–30 nm, except for a small number of aggregations. It is well known that the nanopowder is featured with high diffusion coefficient, high surface energy and low melting point, which are beneficial for rare-earth reacting with boron to form hexaborides at lower sintering temperature.

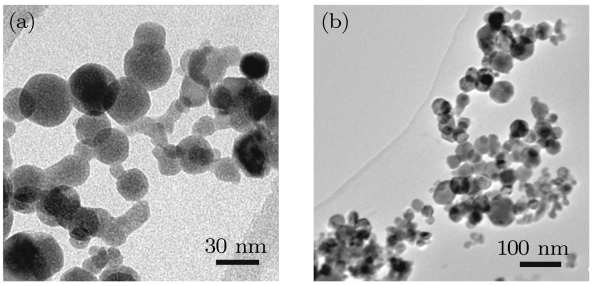


Fig. 1. TEM images of the NdH_2 and the GdH_2 nanopowders. (a) NdH_2, (b) GdH_2.

3.2. Phase and crystal structure identification of the sintered sample

The XRD patterns of the polycrystalline $(Nd_xGd_{1-x})B_6$ bulks with different Nd contents are presented in Fig. 2. It can be seen from Fig. 2(a) that

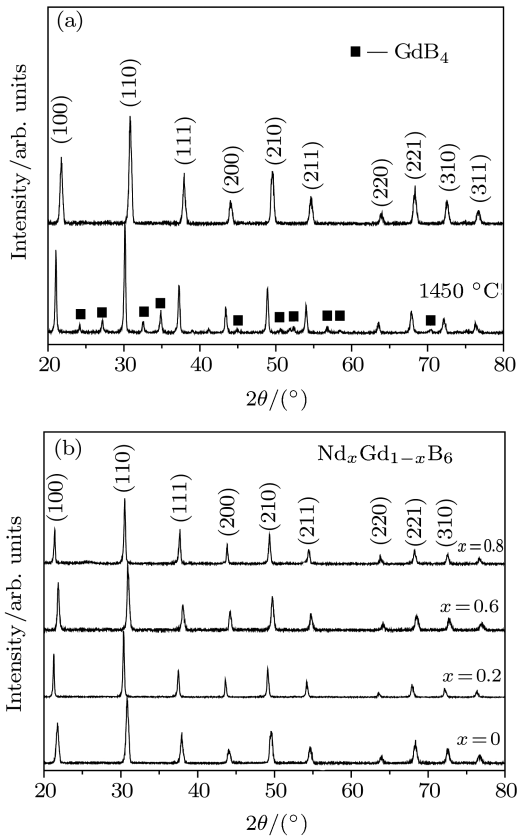


Fig. 2. XRD patterns of (a) GdB_6, (b) $(Nd_xGd_{1-x})B_6$ (x = 0, 0.2, 0.6, 0.8) prepared by the SPS method at 1500 °C under 50 MPa.

all diffraction patterns can be assigned to a large GdB_6 main phase combined with a GdB_4 impurity phase sintered at 1450 °C with P4/mbm symmetry. When the sintering temperature increases up to 1500 °C, the single phase GdB_6 is obtained without the GdB_4 impurity. This indicates that the reaction temperature of B and Gd to form GdB_6 is 1500 °C under the sintering pressure of 50 MPa. According to our previous investigations,[16,17] this reaction temperature is higher than that of the fabrication of LaB_6 and CeB_6 under the same sintering pressure. Figure 2(b) shows the XRD patterns of the $(Nd_xGd_{1-x})B_6$ (x = 0, 0.2, 0.6, 0.8) sintered at 1500 °C under 50 MPa. The XRD analysis shows that all sintered samples with various neodymium dopings are in the single phase with space group Pm-3m, which indicates that the Nd atoms randomly substitute the Gd atoms. The refined lattice parameters obtained by fitting the measured XRD patterns with standard structure models, which was performed by using material studio 4.0, are given in Table 1. It can be clearly seen that the Nd doping leads to a lattice expansion, which is consistent with the fact that the substitute ionic radius of Nd^{3+} (0.99 Å) is larger than that of Gd^{3+} (0.94 Å). Storms[10] reported that the lattice parameters of hexaborides are related to the effective work function and the larger the lattice constant is, the lower the effective work function is. The chemical purities of all sintered samples measured by XRF are above 99.9% as shown in Table 1.

Table 1. The partial properties of sintered $(Nd_xGd_{1-x})B_6$ samples.

$(Nd_xGd_{1-x})B_6$	Purity/%	Lattice constant/Å	Relative density/%	Vickers hardness/kg·mm^{-2}
GdB_6	99.93	4.099	97. 5	2091
$Gd_{0.8}Nd_{0.2}B_6$	99.93	4.113	96.1	2310
$Gd_{0.4}Nd_{0.6}B_6$	99.91	4.120	96.3	2285
$Gd_{0.2}Nd_{0.8}B_6$	99.95	4.126	95.2	2319

3.3. Mechanical property of the sintered sample

The relative densities of the $(Nd_xGd_{1-x})B_6$ (x = 0, 0.2, 0.6, 0.8) bulks are shown in Table 1. It indicates that the high relative density (> 95%) $(Nd_xGd_{1-x})B_6$ ceramics can be obtained by the SPS method. It was reported that the relative densities of NdB_6[1] and GdB_6[11] prepared by the traditional solid phase hot-pressing method were about 68% and 80%, respectively, indicating that the approach was ineffective for full densification. Therefore, the typical liquid reactive SPS mechanism leads to a promoting consolidation procedure. When the sintering temperature is in the range of 729 °C–883 °C, a dehydrogenation reaction[16,17] occurs. The NdH_2 and the GdH_2 form the Nd, Gd nanopowder and the H_2 gas. When the sintering temperature increases up to 1500 °C, the liquid phase Nd and Gd soak and react with the boron powder to form the single phase hexaboride (see Fig. 2). The melting points of Nd and Gd are 1024 °C and 1313 °C, respectively. Obviously, the emergence of liquid phase promotes the sintering by enhancing the rate of mass transport of solid phase boron and inducing the grain rearrangement, which are beneficial for improving the densification. Hence the liquid reactive SPS in situ sintering method is superior to the traditional hot-pressing method. The whole sintering process can be summarized in the above mentioned chemical reaction formula. It can be also found from Table 1 that the Vickers hardnesses of all sintered bulks maintain higher values and the maximum value reaches 2319 kg/mm^2. This may result from the enhancement of the sample densification and the small grain size, which is shown in Fig. 3.

3.4. Electron backscatter diffraction analysis of the grain

Figure 3 shows the EBSD orientation maps of polished $(Nd_xGd_{1-x})B_6$ (x = 0, 0.6, 0.8) bulks. The colors represent the crystallographic orientations according to the inverse pole figure (IPF) shown in the inset. The grain size is in the range from 2 to 5 μm, except for a small quantity of large grains. This result is consistent with the fracture surface observation of the scanning electron microscope.

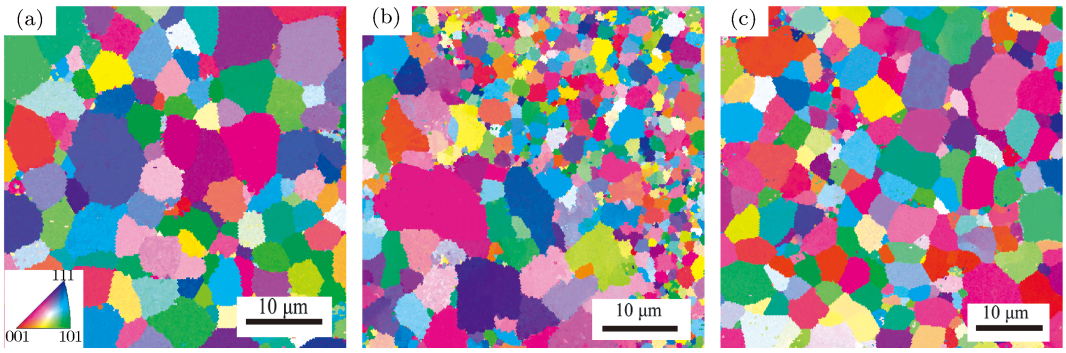


Fig. 3. (colour online) The orientation maps for normal direction of bulk $(Nd_xGd_{1-x})B_6$. (a) $x = 0$, (b) $x = 0.6$, (c) $x = 0.8$.

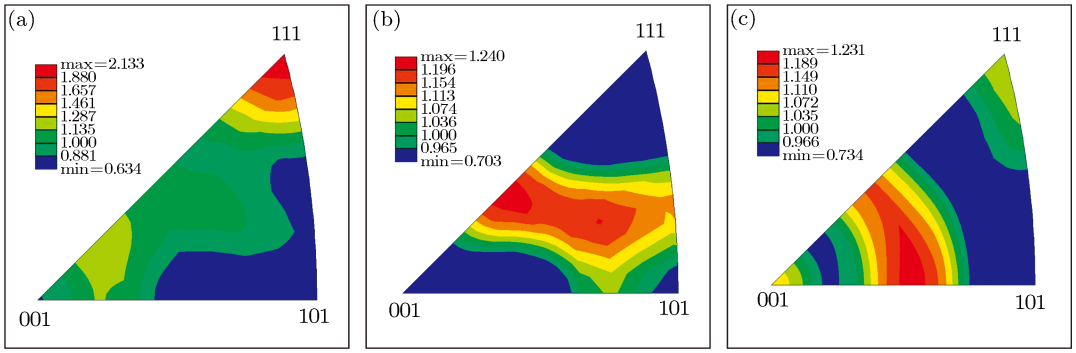


Fig. 4. (colour online) The inverse pole figures of bulk $(Nd_xGd_{1-x})B_6$. (a) $x = 0$, (b) $x = 0.6$, (c) $x = 0.8$.

Figure 4 shows the inverse pole figures, where the color depth indicates the pole area density. It can be seen that the GdB_6 is mainly composed of (111) fiber texture, the $Gd_{0.4}Nd_{0.6}B_6$ is mainly composed of (211) and (527) fiber texture and $Gd_{0.2}Nd_{0.8}B_6$ are mainly composed of (210) fiber texture. According to previous investigations,[18,19] the work functions (Φ) of hexaborides are related to their surfaces: the order of Φ for different surfaces was $\Phi_{(310)} < \Phi_{(210)} < \Phi_{(100)} < \Phi_{(110)} < \Phi_{(111)} < \Phi_{(211)}$. Therefore, it is predicted that the bulk $Gd_{0.2}Nd_{0.8}B_6$ with (210) fiber texture will have superior emission properties.

3.5. Thermionic emission properties of the $(Nd_xGd_{1-x})B_6$ ($x = 0$, 0.2, 0.6, 0.8)

The thermionic emission current density of $(Nd_xGd_{1-x})B_6$ ($x = 0$, 0.2, 0.6, 0.8) was measured with voltages up to 1000 V at various cathode temperatures (from 1673 K to 1873 K). The results are shown in Fig. 5. It can be seen from Fig. 5(a) that with the increase of the applied voltage, the emission current density of GdB_6 at 1673 K increases and its maximum value is 0.37 A/cm^2. When the temperature increases to 1773 K and to 1873 K, the maximum values of the emission current density are 2.76 and 11 A/cm^2, respectively. The measured emission current density of the GdB_6[11] prepared with the traditional method is found to be only 0.00042 A/cm^2 with the voltage of 1400 V at 1700 K, which is much smaller than that obtained in this study. The increase of the emission current should be attributed to the high densification of the SPS sintering, which improves the electron transport and leads to the reduction of the work function. Therefore, the improved mechanical and emission properties of materials result from the enhancement of the densification of hexborides, which is expected. Figures 5(b)–5(d) show the emission current densities of the $(Nd_xGd_{1-x})B_6$ with $x = 0.2$, 0.6 and 0.8. It can be seen that when the Nd doping contents are 20 and 60 at%, there is an increasing tendency in the emission current density and the maximum emission current density increases from 11.15 A/cm^2 to 11.45 A/cm^2 at 1873 K. Furthermore, when the doping content is 0.8, the maximum emission current density increases to 16.30 A/cm^2 at 1873 K and the maximum values at 1773 K and 1673 K are also higher than those of other contents. This result

is consistent with our prediction based on the EBSD. Thus, it is concluded that the emission current density of GdB_6 should be improved with the increase of the doping content

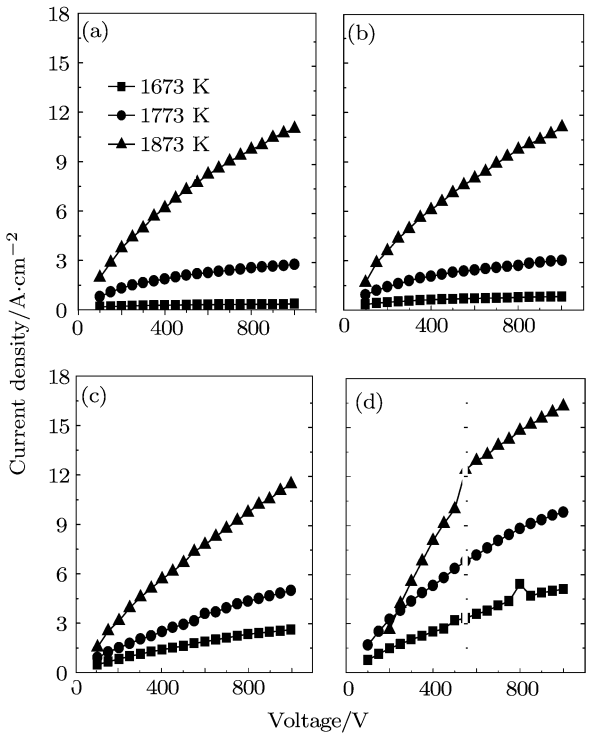


Fig. 5. The dependence of $(Nd_xGd_{1-x})B_6$ emission current density on the doping content with voltages up to 1000 V at various cathode temperatures. (a) $x = 0$, (b) $x = 0.2$, (c) $x = 0.6$, (d) $x = 0.8$.

3.6. Magnetic properties of the $(Nd_xGd_{1-x})B_6$ ($x = 0.2$, 0.6, 1)

The temperature dependence of the magnetization of the $(Nd_xGd_{1-x})B_6$ bulks with $x = 0.2$, 0.6 and 1 measured with increasing and decreasing temperature in a field of 20 mT is shown in Fig. 6. It can be seen that the magnetic phase transition (from antiferromagnetism to paramagnetism) of NdB_6 takes place at about $T_N = 7.95$ K (T_N is the Néel temperature). Same results [2] have been observed in a single crystal NdB_6 with an A-type collinear antiferromagnetic structure below $T_N = 8$ K. The magnetic phase transition temperature of the $(Gd_{0.4}Nd_{0.6})B_6$ bulk is about $T_N = 5.85$ K and the Néel temperature of the $(Gd_{0.8}Nd_{0.2})B_6$ bulk is lower than 5 K. Thus, we can deduce that with the increase of the Nd content, the magnetic phase transition temperature increases. The increase of the Néel temperature should be attributed to the enhancement of magnetic interactions between Nd and Gd moments and between Nd and Nd moments.[21]

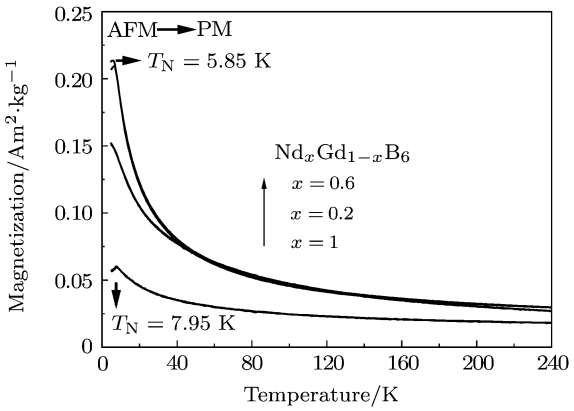


Fig. 6. Temperature dependence of the magnetization of $(Nd_xGd_{1-x})B_6$ with $x = 0.2$, 0.6, 1 measured in a field of 20 mT.

4. Conclusions

The high densified polycrystalline $(Nd_xGd_{1-x})B_6$ have been prepared by SPS in situ sintering the GdH_2, NdH_2 and B powder in an oxygen free system. The typical liquid reactive SPS mechanism is useful to attain the grain preferred orientation and the excellent mechanical properties. The emission current density of $(Nd_xGd_{1-x})B_6$, which is much higher than that obtained in the traditional method, increases linearly with the increase of the Nd doping content. Furthermore, the magnetic phase transition temperature increases with the increase of the Nd content. It can be concluded that the SPS technique is a suitable method for synthesizing high density rare-earth hexaborides with excellent properties.

References

[1] Nishitani R, Aono M, TanaKa T, Kawai S, Iwasaki H, Oshima C and Nakamura S 1980 *Surf. Sci.* **95** 341
[2] Futamoto M, Nakazawa M and Kawabe U 1980 *Surf. Sci.* **100** 470
[3] Lafferty J M 1951 *J. Appl. Phys.* **22** 299
[4] Swanson L W and McNeely D R 1979 *Surf. Sci.* **83** 11
[5] Davis P R, Gesley M A, Schwind G A and Swanson L W 1989 *Appl. Surf. Sci.* **37** 381
[6] Samwer K and Winger K 1976 *Z. Phys.* B **25** 269
[7] Mccarthy C M and Tompson C W 1980 *J. Phys. Chem. Solids* **41** 1319

[8] Reiffers M, Sebek J, Santava E, Pristas G and Kunii S 2006 *Phys. Stat. Sol.* (b) **243** 313

[9] Luca S E, Amara M, Galera R M, Givord F, Granovsky S, Isnard O and Beneu B 2004 *Physica* B **350** E39

[10] Storms E K 1981 *J. Appl. Phys.* **52** 2961

[11] Storms E K and Mueller B A 1981 *J. Appl. Phys.* **52** 2966

[12] Schmidt P H and Joy D C 1978 *J. Vac. Sci. Technol.* **15** 1809

[13] Li Z C, Lu W, Dong X L Zhou F and Zhao Z X 2010 *Chin. Phys.* B **19** 086101

[14] Yun J N, Zhang Z Y Yan J F and Deng Z H 2010 *Chin. Phys.* B **19** 017101

[15] Long X, Li X, Lin P T, Cheng X W, Liu Y and Cao C B 2010 *Chin. Phys.* B **19** 027202

[16] Zhou S L, Zhang J X, Liu D M and Bao L H 2009 *J. Inorganic Mater.* **24** 793 (in Chinese)

[17] Zhou S L Zhang J X, Liu D M, Lin Z L, Huang Q Z, Bao L H, Ma R G and Wei Y F 2010 *Acta Mater.* **58** 4978

[18] Uijttewaal M A, de Wijs G A and Groot R A 2006 *J. Phys. Chem.* B **110** 18462

[19] Gesley M and Swanson L W 1984 *Surf. Sci.* **146** 589

[20] Westrum J E F andrews J T S, Justice B H and Johnson D A 2002 *J. Chem. Thermod.* **34** 239

[21] Dai D S and Qian K M 1987 *Ferromagnetics* (1st ed) (Beijing: Science Press) pp. 147–150